Local Activation Time Estimation in Atrial Electrograms Using Cross-Correlation over Higher-Order Neighbors

Kolling, B.; Abdi, B.; Groot, N.M.S. de; Hendriks, R.C.

Publication date
2020

Document Version
Final published version

Published in
28th European Signal Processing Conference (EUSIPCO 2020)

Local Activation Time Estimation in Atrial Electrograms Using Cross-Correlation over Higher-Order Neighbors

Bart Kölling*, Bahareh Abdi*, Natasja M.S. de Groot†, and Richard C. Hendriks*

*Circuits and Systems (CAS) Group, Delft University of Technology, the Netherlands
†Department of Cardiology, Erasmus University Medical Center, the Netherlands
Email: * bkolling2@gmail.com, *{b.abdikivanani, r.c.hendriks}@tudelft.nl, †n.m.s.degroot@erasmusmc.nl

***Abstract*—Atrial electrograms are often used to gain understanding on the development of atrial fibrillation (AF). Using such electrograms, cardiologists can reconstruct how the depolarization wave-front propagates across the atrium. Knowing the exact moment at which the depolarization wavefront in the tissue reaches each electrode is an important aspect of such reconstruction. A common way to determine the LAT is based on the steepest deflection (SD) of the individual electrograms. However, the SD annotates each electrogram individually and is expected to be more prone to errors compared to approaches that would employ the data from the surrounding electrodes to estimate the LAT. As electrograms from neighboring electrodes tend to have rather similar morphology up to a delay, we propose in this paper to use the cross-correlation to find the pair-wise relative delays between electrograms. Instead of only using the direct neighbors we consider the array as a graph and involve higher order neighbors as well. Using a least-squares method, the absolute LATs can then be estimated from the calculated pair-wise relative delays. Simulated and clinically recorded electrograms are used to evaluate the proposed approach. From the simulated data it follows that the proposed approach outperforms the SD approach.**

***Index Terms*—local activation time, electrogram, cross-correlation**

I. Introduction

Atrial fibrillation (AF) is a common cardiac arrhythmia which is associated with a high overall risk of mortality [1]. One of the common ways to study the mechanism involved in initiation and progression of AF is through high resolution atrial electrograms recorded by electrode arrays positioned directly on the heart surface during open-chest surgeries [2]. Atrial electrograms are used by cardiologists to reconstruct the depolarization wave-front propagation patterns in the atria that can potentially be used to reveal electropathological substrates related to AF. To provide these propagation patterns, we first need to estimate the exact moment in which the depolarization wavefront in the tissue reaches each electrode. These moments are denoted as local activation times (LATs).

The steepest negative deflection in a unipolar electrogram is known to coincide with the depolarization of the tissue under the electrode and is commonly annotated as the LAT [3]. However, this approach annotates each electrogram individually and is expected to be more prone to errors compared to approaches that would employ the data from the surrounding electrodes to estimate the LAT. Moreover, using purely the derivative of the measured signal to estimate the LAT makes it susceptible to spikes added by noise and other artifacts. To overcome this issue, several techniques have been previously proposed in the literature to improve LATs. A review of which can be found in [4]. Since electrograms are the measurement of the same wavefront at different positions and have rather similar morphology, except for a time shift, we propose to use the cross-correlation to find the pair-wise delays between each electrogram and its neighbors. Existing cross-correlation methods use only the closest neighboring electrodes to create pairs for which delays are calculated, see [5]. The resulting delays between the electrodes then do need to be converted to absolute times.

In this paper the application of the cross-correlation for LAT estimation is further investigated. Specifically, the benefits of not only cross-correlating electrode pairs that are close, but also those with a larger distance are of interest. This is done by creating a framework to define higher-order neighbors while evaluating the electrode array as a graph. The cross-correlation is then applied to pairs of electrodes to estimate the delay in their LATs. Next, a least-squares method is used to transform these relative activation times to absolute LATs. Finally, this method is applied to simulated and clinically recorded electrograms and the results are compared to the steepest deflection method.

II. Methods

A. Definition of higher-order neighbors

The multi-electrode electrogram recording provides spatial information that can be exploited to achieve better LAT estimation. In this study, we present the spatial connections between the electrodes as a graph. The electrodes in our recording array are spaced as a regular square grid. This grid is defined by the adjacency matrix $\boldsymbol{A}$,

$$A_{i,j} = \begin{cases} 1 & \text{if } j \in N(i) \\ 0 & \text{otherwise} \end{cases}, \tag{1}$$

where $i, j \in 1, 2, \ldots, M$ are the electrode's indices, and $N(i)$ contains the neighboring electrodes of electrode i in the grid. Matrix $\boldsymbol{A}$ only represents the connections between neighboring electrodes, or, in other words, one *hop* away in the grid graph. In this paper on LAT estimation, we introduce a new adjacency matrix $\boldsymbol{\Xi}^{(P)}$ where the nodes (electrodes) are connected over at most P hops of the template grid, defined as

$$\boldsymbol{\Xi}^{(P)} = \sum_{p=1}^{P} \boldsymbol{A}^p, \tag{2}$$

where the order P of $\boldsymbol{\Xi}^{(P)}$ determines over what distances the nodes are connected by edges.

B. Cross-correlation of electrograms

We use the normalized cross-correlation (NCC) denoted by $\rho_{(i,j)}(s)$ to determine the time differences (delays) $\hat{\Delta}$ in LATs of electrode pairs. The NCC between two electrograms $x_i(k)$ and $x_j(k)$ as a function of the shift in samples s is calculated as

$$\rho_{(i,j)}(s) = \sum_{k} \frac{(x_i(k) - \mu_i)\,(x_j(k-s) - \mu_j)}{\sqrt{\sigma_i^2 \sigma_j^2}}, \tag{3}$$

where μ_i, μ_j are the means and σ_i^2, σ_j^2 are the variances of $x_i(k)$ and $x_j(k)$, respectively. The delay between electrograms i and j, $\hat{\Delta}_{(i,j)}$, is then estimated as

$$\hat{\Delta}_{(i,j)} = \arg\max_{s} \rho_{(i,j)}(s), \quad \text{for } \Xi_{i,j}^{(P)} \neq 0. \tag{4}$$

C. From delays to absolute times

To estimate the per-electrode LATs, we express the inter-electrode delays $\hat{\Delta}$ as a linear system of the absolute LATs as

$$\begin{bmatrix} \hat{\Delta}_{(1,2)} \\ \hat{\Delta}_{(1,3)} \\ \vdots \\ \hat{\Delta}_{(i,j)} \end{bmatrix} = \begin{bmatrix} \tau_2 - \tau_1 \\ \tau_3 - \tau_1 \\ \vdots \\ \tau_j - \tau_i \end{bmatrix} + \begin{bmatrix} \epsilon_{(1,2)} \\ \epsilon_{(1,3)} \\ \vdots \\ \epsilon_{(i,j)} \end{bmatrix} \tag{5}$$

where τ_i is the true activation time of electrode i and $\epsilon_{(i,j)}$ is the estimation error. Since the time delays are calculated for all the links in the graph represented by $\boldsymbol{\Xi}$, we can use the graph's incidence matrix $\boldsymbol{B}$ of size $M \times L$ to rewrite Eq. (5) as

$$\begin{bmatrix} \hat{\Delta}_{(1,2)} \\ \hat{\Delta}_{(1,3)} \\ \vdots \\ \hat{\Delta}_{(2,3)} \\ \vdots \\ \hat{\Delta}_{(i,j)} \end{bmatrix} = \boldsymbol{B}^T \begin{bmatrix} \tau_1 \\ \tau_2 \\ \tau_3 \\ \vdots \\ \tau_i \\ \vdots \\ \tau_j \end{bmatrix} + \begin{bmatrix} \epsilon_{(1,2)} \\ \epsilon_{(1,3)} \\ \vdots \\ \epsilon_{(2,3)} \\ \vdots \\ \epsilon_{(i,j)} \end{bmatrix}, \tag{6}$$

where the incidence matrix is given by

$$\boldsymbol{B}^T = \begin{bmatrix} -1 & 1 & 0 & 0 & \ldots & 0 & \ldots & 0 \\ -1 & 0 & 1 & 0 & \ldots & 0 & \ldots & 0 \\ \vdots & \vdots & \vdots & \vdots & & \vdots & & \vdots \\ 0 & -1 & 1 & 0 & \ldots & 0 & \ldots & 0 \\ \vdots & \vdots & \vdots & \vdots & & \vdots & & \vdots \\ 0 & 0 & 0 & 0 & \ldots & -1 & \ldots & 1 \end{bmatrix}. \tag{7}$$

The system in vector form can be represented as

$$\boldsymbol{d} = \boldsymbol{B}^T \boldsymbol{\tau} + \boldsymbol{e} \tag{8}$$

where $\boldsymbol{\tau}$ of size $M \times 1$ contains the absolute LATs, and $\boldsymbol{d}$ and $\boldsymbol{e}$ of size $L \times 1$ contain the delays and the estimation error, respectively. Note that for a connected graph, the rank of the incidence matrix $\boldsymbol{B}$ is one less than its maximum rank, in this case the rank is $M-1$. Therefore Eq. (8) is rank deficient and thus under-determined.

To estimate the LATs in $\boldsymbol{\tau}$, we assume the error to be zero-mean homoscedastic, so

$$E[\boldsymbol{e}] = \boldsymbol{0}, \quad \text{Cov}(\boldsymbol{\epsilon}) = c\boldsymbol{I} \tag{9}$$

where $0 \leq c < \infty$. We can now use the Gauss-Markov theorem [6] to derive the best linear unbiased estimator (BLUE), also called the ordinary least squares (OLS) estimator, to find the absolute LATs $\hat{\boldsymbol{\tau}}$, which is,

$$\hat{\boldsymbol{\tau}} = (\boldsymbol{B}\boldsymbol{B}^T)^{-1}\boldsymbol{B}\boldsymbol{d}. \tag{10}$$

Since $\boldsymbol{B}^T$ is not full rank, this cannot be solved directly. To overcome this issue, we can use the Moore-Penrose inverse [7] of matrix $\boldsymbol{B}^T$, i.e., $(\boldsymbol{B}^T)^\dagger$, to find the solution

$$\hat{\boldsymbol{\tau}} = (\boldsymbol{B}^T)^\dagger \boldsymbol{d}. \tag{11}$$

This pseudoinverse can be calculated for rank-deficient matrices using the singular value decomposition (SVD).

III. Results

In this section we present results based on simulated electrograms in Sec. III-A, as well as results based on clinical measurements in Sec. III-B.

A. Simulated electrograms

We use the approach described in [8] to generate simulated electrograms, which uses the Courtemache model of the human atrial myocytes [9], together with the mono-domain reaction-diffusion model of the atrial action potential [10] to generate simulated electrograms. The cells are assumed to be on a 2D uniform square grid with a spacing Δx and the electrode array is assumed to be positioned on a parallel plane of the cells and at a constant height.

Two sets of simulated tissues were used to generate simulated electrograms. Tissue **T1**, **T2** and **T3**, whose conductivity maps are shown in the first row of Fig. 1, have specific patterns of blocking or slow conduction. Theses patterns are less realistic, but are used to exaggerate the differences between the methods of LAT estimation. We also use more

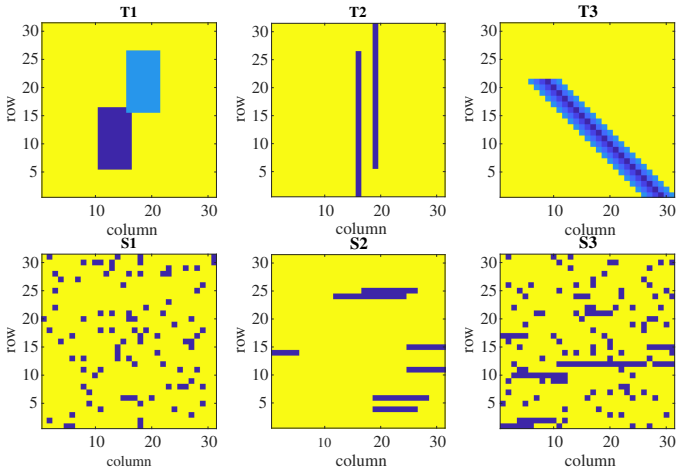

Fig. 1. The simulated conductivity maps with different patterns of blocks and slow conduction for generating simulated electrograms.

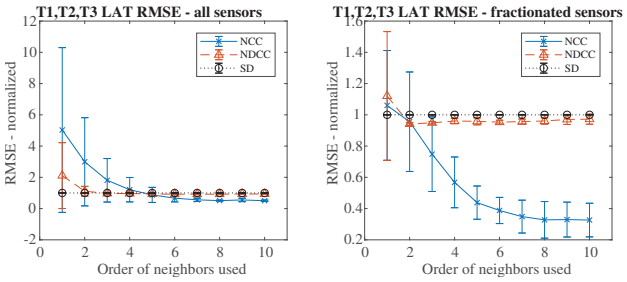

Fig. 2. The normalized RMSE in LAT estimation by different methods for simulated electrograms using the tissue patterns **T1**, **T2**, **T3**. The error bars indicate the standard deviation. Left: error in LAT estimation for all electrograms. Right: error in LAT estimation for electrodes with fractionated electrograms only.

TABLE I

THE RMSE (IN MS) IN LAT ESTIMATION BY DIFFERENT METHODS FOR SIMULATED ELECTROGRAMS USING THE TISSUE PATTERN **T1**, **T2**, **T3** IS SHOWN. THE FIRST THREE ROWS SHOW THE PERFORMANCE OVER ALL ELECTRODES, AND THE BOTTOM THREE ROWS (DENOTED BY (F)) FOR ELECTRODES WITH FRACTIONATED ELECTROGRAMS ONLY.

	SD	**NCC-1**	**NCC-10**	**NDCC-1**	**NDCC-10**
T1	2.41	3.00	**1.27**	2.21	2.26
T2	11.54	32.17	**5.26**	10.02	11.03
T3	0.93	10.31	**0.49**	4.24	0.85
T1 (f)	8.66	6.60	**2.41**	7.87	8.24
T2 (f)	27.69	40.08	**12.46**	23.72	26.47
T3 (f)	3.44	3.34	**0.87**	5.49	3.47

realistic conductivity maps, shown in the second row of Fig. 1, to generate simulated electrograms. These are examples of the different patterns that mimic decoupling of conduction between areas of atrial tissue [11]. This can be caused by excessive deposition of collagen due to fibrosis in the heart. As can be seen in Fig. 1, **S1** contains spots of no conduction, **S2** contains lines of no conduction and **S3**, contains a combination of both. Note that we use 10 randomly generated realizations of each pattern and use their average results for consistent performance evaluation.

To compare the result of LAT estimation, we use three different methods: (i) The steepest deflection (SD) method, (ii) the normalized cross-correlation on the electrograms of Pth order neighbors (i.e., with a maximum of P hops), referred to as NCC-P, and (iii) the normalized cross-correlation on the first temporal derivative of the electrograms of Pth order neighbors (i.e., with a maximum of P hops), referred to as NDCC-P. After estimating the delays using NCC and NDCC, we use the OLS method in Eq. (10) to obtain the LATs. In addition to the error in LAT estimation averaged over all electrograms, we also estimate the error in fractionated electrograms only (those having multiple negative deflections).

Fig. 2 shows the resulting root mean square error (RMSE) and standard deviation, averaged over the datasets **T1**, **T2**, and **T3**. The RMSE is normalized with respect to the RMSE of the SD approach, therefore the RMSE of the SD equals one for every tissue pattern. For the NCC-P and NDCC-P approach we show the performance as a function of P. That is, an increased order of neighbors P for the connectivity graph $\Xi^{(P)}$. As can be seen, using higher order neighboring pairs (larger P), decreases the errors in LAT estimation methods. This implies increasing P in $\Xi^{(P)}$ and thus increasing the distance in the grid graph over which cross-correlations are calculated. The NCC method's error keeps decreasing well below the error of the SD method. This happens when taking all electrodes into account, but also when calculating the RMSE only for electrodes where the signal is fractionated as shown in the right subgraph of Fig. 2. The NDCC method's error does decrease when higher-order neighbors are used but it converges to a value only marginally below the error of the SD. It seems the NDCC method does benefit from having a larger number of delays to calculate the LAT, but not as much as the NCC method. The first temporal derivative of the data, as used in SD and NDCC, can be seen as a high-pass filtered version of the original electrogram. The high frequency components, such as steep deflections, will thus be more prominent than the low frequency components. The cross-correlation will then focus on these steep deflections instead of on the complete electrogram and the resulting estimate is in the end similar to that of the SD method. Table I provides an overview of non-normalized RMSEs (in ms) for the individual **T** patterns.

Fig. 3 shows the results of LAT estimation using the different approaches for LAT applied on **S3**. The same trend as for the **T**-type tissues is visible. The performance on the other **S** sets is similar to that of **S3**. Table II shows the RMSE (in ms) in LAT estimation for each method. As can be seen in all tissue patterns, using the higher order neighbors to determine delays using the NCC methods gives the best performance in every simulation examined.

B. Clinically recorded electrograms

For an evaluation using clinical recordings, we use an electrode array to record electrograms from the surface of human atria during open chest surgeries. The array is manually placed by the surgeon at different locations on the atria to provide an almost complete mapping of the whole atria. The

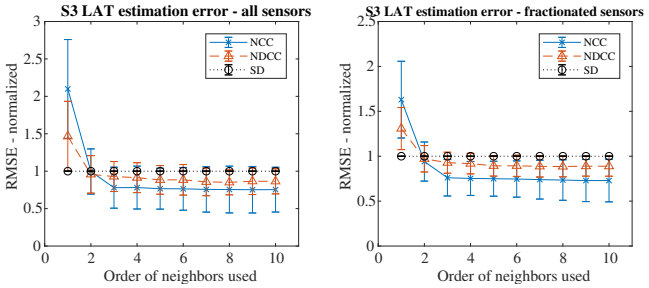

Fig. 3. Normalized RMSE for 10 randomly generated tissues with the **S3** pattern. The error bars indicate the standard deviation. Left: error in LAT estimation for all electrograms. Right: error in LAT estimation for electrodes with fractionated electrograms only.

TABLE II
THE MEAN RMSE (IN MS) FOR THE 10 RANDOMLY GENERATED TISSUES WITH THE **S1**, **S2** AND **S3** PATTERNS. THE FIRST THREE ROWS SHOW THE PERFORMANCE OVER ALL ELECTRODES, AND THE BOTTOM THREE ROWS (DENOTED BY (F)) FOR ELECTRODES WITH FRACTIONATED ELECTROGRAMS ONLY.

	SD	**NCC-1**	**NCC-10**	**NDCC-1**	**NDCC-10**
S1	0.69	0.82	**0.40**	0.85	0.44
S2	1.26	3.16	**0.89**	2.11	1.08
S3	1.63	3.07	**1.06**	2.09	1.29
S1 (f)	1.27	1.31	**0.88**	1.44	0.98
S2 (f)	2.73	4.55	**1.94**	3.73	2.47
S3 (f)	2.64	4.12	**1.83**	3.37	2.31

electrode array used for our measurements consisted of 8×24 electrodes with inner-electrode distance of 2 mm resulting in 192 signal channels. The four electrodes on the corners are not used for epicardial measurements, but serve other purposes. The recorded signals are amplified with a gain of 1000, bandpass filtered (0.5-400 Hz), sampled at 1 kHz and quantized with 16 bits. Pleas see [2] for more details on the array specification and the mapping procedure.

To evaluate the performance of our proposed approach in LAT estimation of clinically recorded electrograms, we use the SD approach and the proposed NCC-10, which provided the best results in the last section. Since we do not have access to the true LATs of the clinically recorded electrograms, we only compare the results of the different approaches with each other while no direct measure of their accuracy will be presented. We use two sets of electrograms recorded from two patients undergoing coronary artery bypass surgery containing one atrial beat during sinus rhythm (SR) in a time window of 200 ms and discuss the results.

The resulting LATs of the first electrogram array, recorded from the left pulmonary vein site, is presented in Fig. 4. As can be seen, in the highlighted electrodes (column 20, row 4 and 5), using the SD results in an 8 ms difference in LAT between these two electrodes, while using NCC-10 results in a 3 ms delay between these electrodes. The middle-top subplot of Fig. 4 also shows the electrogram for the sensor at column 20 and row 5 (solid line) and for comparison also the electrogram for the sensor at column 20 and row 4 (dotted line). The right-top subplot of Fig. 4 shows the same electrograms, but then

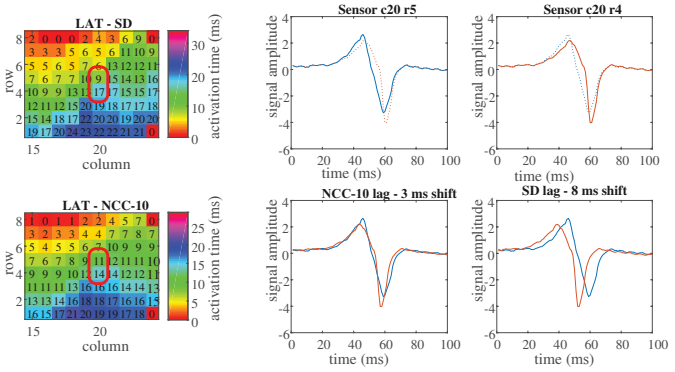

Fig. 4. The per electrode LATs (in ms) estimated using SD (top left) and NCC-10 (bottom left). Top-middle and top-right the highlighted electrograms and bottom-middle and bottom-right their shifted version with respect to the estimated LATs.

the electrogram for the sensor at column 20 and row 4 is highlighted (solid line) and the electrogram for the sensor at column 20 and row 5 (dotted line) is given for comparison. The middle-bottom and middle-right subplots show the same electrograms, but now shifted in time, to compensate for the delays estimated by NCC-10 and SD, respectively. As can be seen, the signals are more synchronized when using NCC-10 which can potentially suggest a more accurate LAT estimation.

The second electrogram array used in this study, is recorded from the left atrium of a patient with a history of paroxysmal AF. The results are presented in Fig. 5 in a similar way as in Fig. 4. The signals of the two highlighted electrodes (row 7, column 11 and 12) are compared in the top-middle and top-right subplot. The top-left and bottom-left subplots show that SD detects a difference of 9 ms in the LATs, while NCC-10 detects a difference of 4 ms, respectively. As before, the signals are shifted according to the estimated delays and the resulted plots are also shown in Fig. 5 (bottom-middle and bottom-right subplot). Because the point of steepest deflection is at the beginning of the downward slope in one electrode and at the end of the slope in another electrode, SD detects a larger delay. On the other hand, NCC-10 matches the entire signals of many electrograms in the array with each other, which results in a smaller delay estimation.

IV. CONCLUSIONS

In this paper we introduced a new approach for LAT estimation in atrial electrograms by using normalized cross-correlation between the higher-order neighbors in electrode pairs. We then compared the performance of our proposed approach with the traditional steepest deflection approach using simulated electrograms. The results show that using normalized cross-correlation over higher order neighbors improves the performance of LAT estimation and out-performs the reference method, which is based on the steepest deflection. Moreover, we provided examples of applying our proposed method and the reference method (steepest deflection) on

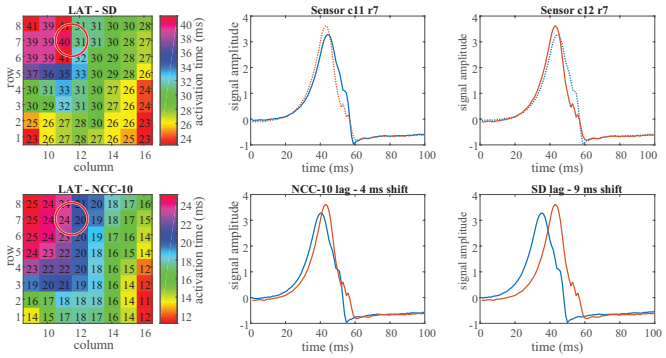

Fig. 5. The per electrode LATs (in ms) estimated using SD (top left) and NCC-10 (bottom left). Top-middle and top-right the highlighted electrograms and bottom-middle and bottom-right their shifted version with respect to the estimated LATs.

clinically recorded electrograms and discussed the distinct differences in the results. This showed potential advantages of cross-correlation over higher order neighbors when determining the delay between local activation times.

REFERENCES

[1] A. D. Krahn, J. Manfreda, R. B. Tate, F. A. Mathewson, and T. E. Cuddy, "The natural history of atrial fibrillation: Incidence, risk factors, and prognosis in the manitoba follow-up study," *The American Journal of Medicine*, vol. 98, no. 5, pp. 476 – 484, 1995.

[2] A. Yaksh, L. J. van der Does, C. Kik, P. Knops, F. B. Oei, P. C. van de Woestijne, J. A. Bekkers, A. J. Bogers, M. A. Allessie, and N. M. de Groot, "A novel intra-operative, high-resolution atrial mapping approach," *Journal of Interventional Cardiac Electrophysiology*, vol. 44, no. 3, pp. 221–225, Dec 2015.

[3] M. S. Spach, R. C. Barr, G. A. Serwer, J. M. Kootsey, and E. A. JOHNSON, "Extracellular potentials related to intracellular action potentials in the dog purkinje system," *Circulation research*, vol. 30, no. 5, pp. 505–519, 1972.

[4] C. D. Cantwell, C. H. Roney, F. S. Ng, J. H. Siggers, S. Sherwin, and N. S. Peters, "Techniques for automated local activation time annotation and conduction velocity estimation in cardiac mapping," *Computers in biology and medicine*, vol. 65, pp. 229–242, 2015.

[5] R. Dubois, S. Labarthe, Y. Coudière, M. Hocini, and M. Haïssaguerre, "Global and directional activation maps for cardiac mapping in electrophysiology," in *Computing in Cardiology*, 2012, pp. 349–352.

[6] S. M. Kay, *Fundamentals of statistical signal processing*, ser. Prentice Hall signal processing series. Upper Saddle River, NJ: Prentice Hall PTR, 1993, vol. Volume I: Estimation Theory.

[7] G. H. Golub and C. F. Van Loan, *Matrix computations*. JHU press, 2012, vol. 3.

[8] B. Abdi, R. C. Hendriks, A.-J. van der Veen, and N. M. de Groot, "A compact matrix model for atrial electrograms for tissue conductivity estimation," *Computers in Biology and Medicine*, 2019.

[9] M. Courtemanche, R. J. Ramirez, and S. Nattel, "Ionic mechanisms underlying human atrial action potential properties: insights from a mathematical model," *American Journal of Physiology-Heart and Circulatory Physiology*, vol. 275, no. 1, pp. H301–H321, 1998.

[10] R. Plonsey and R. C. Barr, *Bioelectricity: a quantitative approach*. Springer Science & Business Media, 2007.

[11] M. A. Allessie, N. M. S. de Groot, R. P. M. Houben, U. Schotten, E. Boersma, J. L. Smeets, and H. J. Crijns, "Electropathological substrate of long-standing persistent atrial fibrillation in patients with structural heart disease: longitudinal dissociation," *Circulation: Arrhythmia and Electrophysiology*, vol. 3, no. 6, pp. 606–615, 2010.